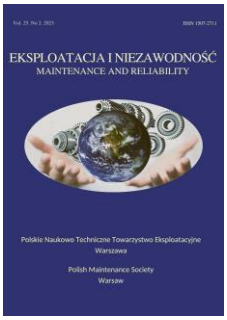

Eksploatacja i Niezawodnosc – Maintenance and Reliability
Volume 28 (2026), Issue 4
journal homepage: http://www.ein.org.pl

Article citation info:
Hou Y, Tang J, Pang P, Yin Q, Zhang J, Zhang H, Research on intelligent fault diagnosis method of rotating machinery under noisy environment based on graph neural network, Eksploatacja i Niezawodnosc – Maintenance and Reliability 2026: 28(4) http://doi.org/10.17531/ein/219156

Research on intelligent fault diagnosis method of rotating machinery under noisy environment based on graph neural network

Indexed by: Web of Science Group

Yinchuan Hou[a], Jian Tang[a,*], Pengfei Pang[a], Qin Yin[a], Jing Zhang[a], Hao Zhang[a]

[a] The Army Engineering University of the PLA of China, China

Highlights

- Integrate multi-channel signals and utilize complementarity to suppress noise, breaking through the limitations of a single channel.
- Introduce the envelope activation function to enhance shock, sparse features and suppress noise.
- The cross-correlation function graph outperforms traditional distance measurement methods under strong noise.
- Embed a time-shift compensation mechanism to capture phase offset and improve time-domain alignment accuracy.

Abstract

In response to the challenges of fault diagnosis for industrial equipment in high-noise environments, this study proposes an improved graph neural network model that combines envelope activation and cross-correlation function. This model first enhances single-channel feature extraction and anti-noise ability through an improved independent parallel one-dimensional convolution structure and envelope activation operation, achieving single-channel noise suppression and feature extraction; then, it uses the time-domain cross-correlation function to construct a topological graph structure between channels, highlighting the essential correlations of multi-channel signals, and realizes multi-channel feature fusion through graph convolution networks. Experimental results on the public bearing dataset show that proposed model has high classification accuracy, superior anti-noise performance, and good generalization ability in high-noise environments.

Keywords
multichannel vibration signal, graph neural network, envelope activation, cross-correlation function, strong noise working condition

1. Introduction

Fault diagnosis of mechanical equipment is a core link to ensure production safety and improve operation and maintenance efficiency. By accurately identifying abnormal conditions of equipment, it effectively prevents sudden accidents and optimizes maintenance decisions, becoming an indispensable key guarantee in the process of industrial intelligence [1]. The traditional fault diagnosis methods in the industrial field are mainly based on the use of techniques such as Fast Fourier Transform (FFT), Wavelet transform (WT) [2], and Empirical Mode Decomposition (EMD) [3] to analyze and process vibration signals. However, with the iterative development of machine learning technology, fault diagnosis has evolved from the traditional methods based on time-frequency feature extraction and shallow statistical modeling to the data-driven intelligent diagnosis paradigm. In the early studies, the shallow neural network models with typical architectures such as BP neural network [4] and Radial Basis Function Network (RBFN) [5] achieved intelligent pattern recognition by capturing the

(*) Corresponding author.
E-mail addresses: Y. Hou (ORCID: 0009-0000-4473-0898) 1342332590@qq.com, J. Tang (ORCID: 0000-0002-2285-4491) lgdx_tj@163.com, P. Pang (ORCID: 0009-0001-4557-9269) lgdx_pangpf@aeu.edu.cn, Q. Yin (ORCID:0009-0003-7218-8372) 108873108@qq.com, J. Zhang (ORCID: 0009-0008-9809-1006) lgdx_zhangj@aeu.edu.cn, H. Zhang (ORCID:0009-0004-8120-9961) maxzhanghao@163.com

nonlinear fault feature representations in vibration signals through an end-to-end learning mechanism. However, the strong noise interference commonly existing in industrial sites (such as mechanical friction noise, electromagnetic coupling noise, etc.) leads to severe distortion of vibration signals. Due to the limited feature representation ability of the above models, the classification accuracy significantly decreases under the condition of low SNR, and the anti-noise robustness urgently needs to be improved.

To overcome the above-mentioned bottlenecks, deep learning technology has gradually become a research hotspot in the field of fault diagnosis [6–14]. Convolutional Neural Network (CNN) [15] is capable of extracting the deep spatial features of vibration signals from the noisy background through local perception and weight sharing mechanisms. Recurrent neural networks (RNN) and their variants (such as LSTM) [16] utilize time-dependent modeling to effectively capture the dynamic evolution laws during the device degradation process. Based on the above model architecture, the academic community has achieved a series of research results, demonstrating significant advantages in improving diagnostic accuracy and anti-noise robustness. Wang et al. [17] proposed an attention-guided joint learning convolutional neural network, integrating fault diagnosis and signal denoising tasks into an end-to-end CNN architecture, and achieving good noise robustness through dual-task joint learning; Guo et al. [18] proposed a model for bearing fault diagnosis under strong noise, which enhances the adaptability of secondary neurons through adaptive gating factors and establishes a connection with learnable weighted autocorrelation to better extract features. Experiments have proved that it has good anti-noise ability and excellent performance. The above research, through multi-layer nonlinear transformation and end-to-end learning strategies, can still maintain a high diagnostic accuracy in a strong noise environment, and the anti-noise performance is significantly improved compared with traditional methods.

However, the above studies mostly focus on the analysis of single-channel vibration signals. In fault diagnosis, relying solely on single-channel vibration signals has significant limitations: On the one hand, single-channel is restricted by the position and direction of sensor distribution points, making it difficult to capture the fault characteristics of the entire equipment domain (such as coupled vibrations of multiple components and fault propagation path information); On the other hand, in a strong noise environment, single-channel signals are prone to noise interference being directly conducted to the diagnostic model due to the limitation of single-point perception, intensifying the distortion risk of effective features. In contrast, multi-channel vibration signals construct information redundancy and spatial correlation through the collaborative perception of multiple sensors, which can significantly enhance the anti-noise ability [19–21]. Ye et al. [22] proposed a multi-sensor residual convolution fusion network, designing three major modules: double-loop residual, spatial channel reconstruction, and global interactive perception fusion. It can effectively fuse the signal characteristics of multiple sensors. Experiments have proved that it has better anti-noise ability. Yan et al. [23] proposed a mechanical multi-sensor fault diagnosis method based on adaptive multi-feature pattern decomposition and multi-attention fusion residual convolutional neural network. Experimental verification shows that this method has more advantages in fault identification and stronger anti-noise robustness than similar technologies.

Although the above model has initially achieved cross-channel feature fusion of multi-channel vibration signals, its essence still belongs to the shallow interaction of multi-channel signal features in the vector space. It fails to effectively fuse the non-Euclidean spatial topological associations among multi-channel sensor entities, restricting the exploration of the essential coupling laws of multi-dimensional vibration signals in complex mechanical systems. This leads to the limitation of the characterization ability of nonlinear interactions among multi-channel signals under complex working conditions, restricting the continuous improvement of anti-noise performance. This bottleneck drives researchers to seek breakthroughs in topology-aware models such as Graph Neural Network (GNN) [24,25].

With its advantages in non-European data processing, GNN has demonstrated remarkable characteristics in the field of graph structure data modeling, providing a new research paradigm for multi-channel vibration signal analysis [26–28]. Li et al. [29] proposed a multi-view graph neural network, constructed multi-views integrating time-domain and frequency-domain features based on Euclidean distance, and

achieved multi-sensor information aggregation and fusion by using graph convolutional blocks and view attention blocks. Experiments proved that its performance was superior. Liu et al. [30] proposed a spatio-temporal frequency graph attention network. By encoding the time-frequency information through the Transformer and combining the spatio-temporal graph attention network to capture the spatio-temporal relationship of multiple sensors, the multi-channel signal feature fusion for fault diagnosis of rotating machinery can be achieved, and a relatively high classification accuracy can still be reached under strong noise conditions. The above GNN variant models conduct feature characterization for the non-Euclidean geometric correlation of multi-channel vibration signals and construct a schema interaction mechanism for cross-channel signal features. However, there is still room for improvement, mainly including:

1. At the graph construction level, the model mainly relies on the distance between vibration signals (such as Euclidean distance) to construct the graph structure, and does not fully integrate the essential characteristics of the signals. This distance-based composition method is prone to noise interference under strong noise conditions, resulting in distortion of node correlation relationships, and further affecting the accurate representation of the spatial relationship of real sensors by the graph structure.
2. At the feature extraction level, the global attention mechanism of the Transformer architecture may cause the attention diffusion problem of key vibration modes, resulting in the change of the fault-sensitive features of the original vibration signal during the encoding process, which restricts the identification accuracy of mechanical fault-sensitive features in a strong noise background.

To overcome the above deficiencies, this paper proposes an improved Graph Convolutional Network model for multi-channel vibration signals based on envelope activation and cross-correlation function mapping strategies (ECGCN) as a fault diagnosis model. The model improvement is mainly reflected in the following two core parts.

1. Single-channel feature extraction: A parallel and independent one-dimensional convolution architecture is constructed. A lightweight single-layer convolution kernel is used to initially extract the vibration signal features of each channel and suppress noise. Envelope activation is adopted to selectively enhance the intrinsic impact components under strong noise interference, achieving feature enhancement of the fault impact components.
2. Multi-channel feature fusion: Design a noise-robust graph topology construction strategy, establish the feature correlation among multi-channel signals based on the integral anti-interference characteristics of the time-domain cross-correlation function, and achieve the fusion of multi-channel vibration signal features through the graph convolutional network to further improve the fault feature representation ability in a noisy background.

The main structure of the article is as follows. Section 1, the introduction part mainly introduces the development history of mechanical fault diagnosis technology and the current situation at home and abroad of the research of deep learning technology in the field of fault diagnosis under the background of strong noise. Section 2 presents the model framework of ECGCN and gives a specific introduction to its theoretical basis. Section 3: Experiments are conducted to verify the superiority of the model and the effectiveness of the improvement strategy. Section 4 summarizes the full text.

2. Improved graph neural network for multi-channel vibration signals

The fault diagnosis framework based on ECGCN is shown in Fig.1. The entire process consists of three core modules: the multi-channel vibration signal acquisition and preprocessing module, the model training module, and the fault classification and pattern recognition module. The innovation focus of this research is on the dual key technologies in the model training stage - feature extraction of single-channel signals and feature fusion of multi-channel signals. Through the collaborative working mechanism of these two modules, an end-to-end diagnostic process from the original vibration signal to the discrimination of equipment status is achieved. Specifically, the feature extraction module is responsible for capturing the fault-sensitive information of each sensor channel, while the feature fusion module builds discriminative feature expressions through cross-channel information interaction. Together, they constitute the core technical architecture of the system. The

following text will elaborate on this in detail.

2.1. Independent and parallel improved convolutional layers

The traditional convolutional neural network consists of convolutional layers, pooling layers, bias terms and activation functions. Research on the mechanism of lightweight CNN feature extraction based on Pang et al. [31]: The pooling layer will compress the time-domain resolution of the signal through down sampling, which may weaken the time-domain characteristics of the fault impulse pulse. The bias term has a significant interference in capturing fault features under the condition of strong background noise. Traditional nonlinear activation functions are prone to introducing non-fault features during the feature extraction process, which may affect the diagnostic results. Inspired by this, the convolutional layer module was improved. As shown in Fig. 2., a three-stage optimization strategy was adopted.

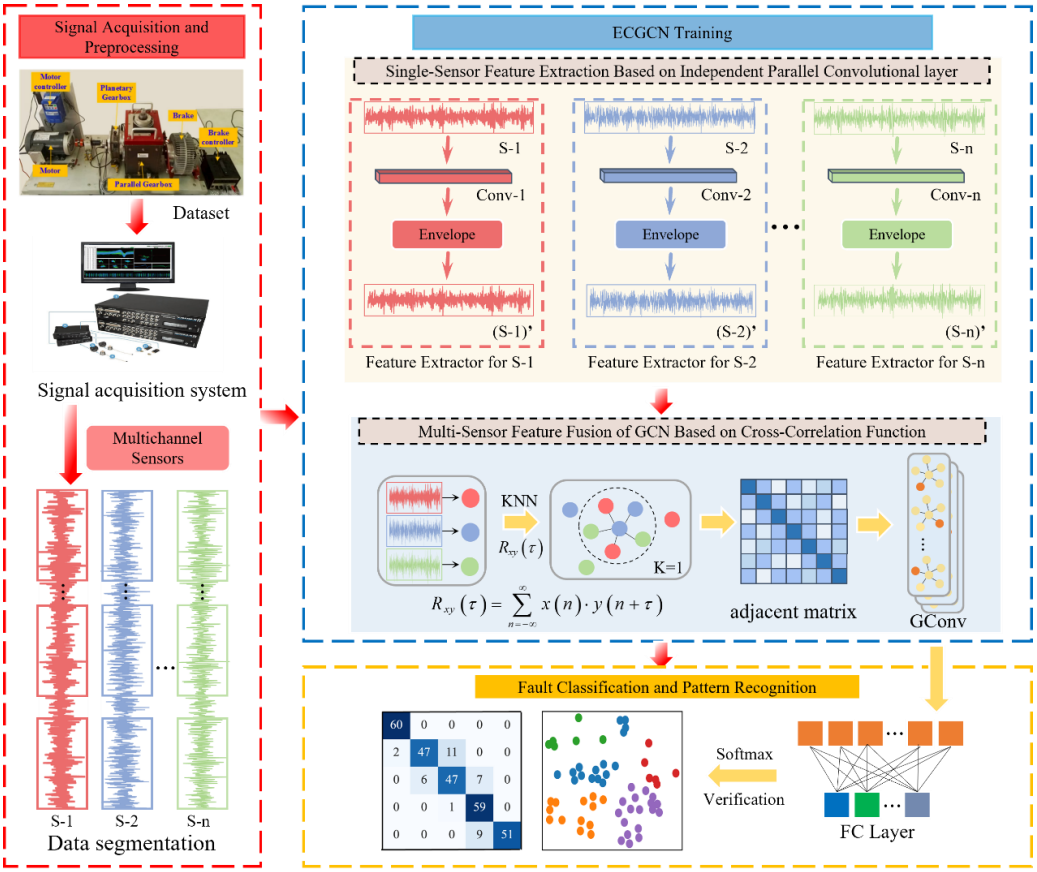

Figure 1. Flowchart of fault diagnosis based on ECGCN.

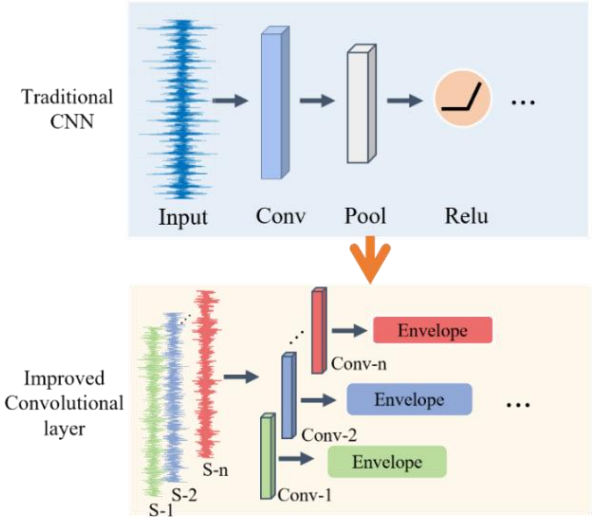

Figure 2. Improved convolutional layer architecture.

1. Structural optimization: Based on the convolutional neural network model, the pooling layer is removed and filling is adopted to maintain the dimensional consistency before and after feature extraction; Discard the bias term to eliminate the influence of noise coupling on feature capture; The traditional nonlinear activation function is removed to avoid extracting the high-order harmonic components irrelevant to the fault. By adopting a single convolutional layer architecture for primary feature extraction, it effectively ensures that only the real fault features are retained in the feature space.

2. Feature domain enhancement: Commonly used activation functions in convolutional neural networks typically include Relu, Sigmoid, and Tanh, etc. However, these activation

functions are not applicable to one-dimensional vibration signals under strong noise conditions, as they introduce non-fault frequency feature components and affect the model's diagnostic results. In this paper, envelope activation is adopted instead of the traditional activation function, that is, the Hilbert transform is performed on the feature vectors output by the convolutional layer and the envelope features on them are extracted. The specific mathematical transformation is as follows:

First, as shown in Eq.(1), perform a Hilbert transform on the feature vector $x(t)$ output by the convolutional layer to obtain its orthogonal components $\hat{x}(t)$.

$$\hat{x}(t) = H[x(t)] = \frac{1}{\pi}\int_{-\infty}^{\infty}\frac{x(\tau)}{t-\tau}d\tau \quad (1)$$

Then, as shown in Eq.(2), based on the Hilbert transform, construct its analytical signal and extract the upper envelope.

$$E_{upper} = |x(t) + j\hat{x}(t)| \quad (2)$$

Which j is an imaginary unit, $|\square|$ representing the modulo operation. The resulting feature E_{upper} is the upper envelope characteristic of the signal.

The envelope activation process is shown in Fig. 3. It can be seen from this that the envelope transformation of characteristic signals can effectively highlight the impact components and modulation modes, which is suitable for the vibration signal analysis of rotating machinery such as bearings and gears, and helps to enhance the model's perception ability of fault characteristics. The features activated by the envelope will participate in the subsequent feature fusion and extraction processes.

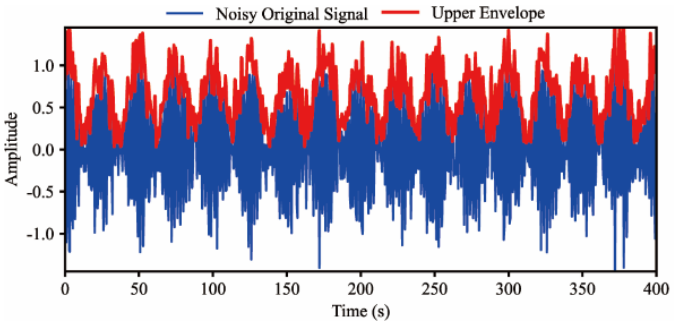

Figure 3. Schematic diagram of envelope activation.

3. Parallel feature extraction: A multi-channel independent parallel improved convolutional layer structure is adopted to extract features from each vibration signal channel respectively. By constructing a parallel convolutional sub-network with non-shared parameters, channe-specific time-frequency feature representation is achieved, effectively preserving the integrity of heterogeneous sensor information and providing a high-discrimination feature input basis for subsequent cross-channel feature fusion.

2.2. Graph construction method based on cross-correlation function

After extracting the features of multi-channel signals based on the improved independent parallel convolutional layer, the graph topology structure is constructed for the enhanced channel features. The multi-scale graph neural network is used for cross-channel feature interaction and hierarchical fusion to achieve further feature enhancement.

For graph convolutional neural networks, the core computation is shown as Eq.(3). Among them, $\boldsymbol{H}^{(l)}$ is the node feature matrix of the lth layer, $\boldsymbol{W}^{(l)}$ is the weight matrix of the lth layer, which is a learnable parameter matrix, σ is the activation function, and $\widehat{\boldsymbol{A}}$ is the adjacency matrix. The adjacency matrix, as one of the key input features of graph convolutional networks, its topological characteristics and data distribution directly affect the training dynamics and generalization ability of the model. During the model optimization process, $\widehat{\boldsymbol{A}}$ dominates the feature propagation path and weight learning direction in the graph convolutional layer by encoding the structured association relationship between nodes. This determines that designing a reasonable construction method for the multi-channel vibration signal graph structure plays a decisive role in improving the performance of the model.

$$\boldsymbol{H}^{(l+1)} = \sigma\left[\left(\boldsymbol{H}^{(l)}, \boldsymbol{A}\right)\cdot \boldsymbol{W}^{(l)} + b^{(l)}\right] \quad (3)$$

Common graph construction methods are based on the K-nearest Neighbor (KNN) algorithm framework and usually adopt the edge generation strategy combining Euclidean Distance(ED) or cosine similarity(CS) with cross-channel ranking screening [27,29,32,33]. The correlation strength between cross-channel samples is measured by ED or CS. Then, adjacent nodes are screened based on similarity ranking. Finally, the top K candidate nodes of cross-channel similarity are directionally connected for the node samples of each channel, thereby establishing an edge structure among multi-channel signal samples.

However, under conditions of strong noise, the composition method based on the above has certain limitations. When the

signal samples $\boldsymbol{x}_i^p$ and $\mathbf{x}_i^q$ from the pth channel and the qth channel are interfered with by the noise n_i^p, n_i^q, the signal x'^p_i and x'^q_i is obtained.

$$\begin{cases} x'^p_i = x_i^p + n_i^p \\ x'^q_i = x_i^q + n_i^q \end{cases} \tag{4}$$

At this time, the ED between the signals from the pth and qth channels is:

$$ED(x'^p_i, x'^q_i) = \sqrt{\sum_{i=1}^{l}(x'^p_i - x'^q_i)^2} = \sqrt{\sum_{i=1}^{l}\left((x_i^p - x_i^q) + (n_i^p - n_i^q)\right)^2} \tag{5}$$

The CS is：

$$CS(x'^p_i, x'^q_i) = \frac{\sum_{i=1}^{l} x'^p_i x'^q_i}{\sqrt{\sum_{i=1}^{l}(x'^p_i)^2}\sqrt{\sum_{i=1}^{l}(x'^q_i)^2}} = \frac{\sum_{i=1}^{l}(x_i^p + n_i^p)(x_i^q + n_i^q)}{\sqrt{\sum_{i=1}^{l}(x_i^p + n_i^p)^2}\sqrt{\sum_{i=1}^{l}(x_i^q + n_i^q)^2}} = \frac{\sum_{i=1}^{l}(x_i^p x_i^q + x_i^p n_i^q + x_i^q n_i^p + n_i^p n_i^q)}{\sqrt{\sum_{i=1}^{l}\left[(x_i^p)^2 + 2x_i^p n_i^p + (n_i^p)^2\right]}\sqrt{\sum_{i=1}^{l}\left[(x_i^q)^2 + 2x_i^q n_i^q + (n_i^q)^2\right]}} \tag{6}$$

Eq.(5) indicates that the ED calculates the absolute distance between two signals in space. Noise will directly increase the amplitude fluctuation of the signals. When the noise intensity is large, it may completely mask the true differences between the signals, causing the calculated distance to lose its effective representation of the original signal relationship. It can be seen from Eq.(6) that when the noise intensity is large enough$(n \gg x)$, the cosine direction representing the signal similarity is mainly dominated by the noise. At this time, the CS approaches zero, is consistent with the similarity of random noise, and is independent of the original signal. Therefore, in a strong noise environment, the construction of the adjacency relationship of multi-channel vibration signals based on ED and CS has essential flaws: it is highly sensitive to noise, and it will undergo a large offset due to the existence of noise. In the process of constructing edges, the correlation of the underlying fault characteristics has not been considered.

The Cross-Correlation Function (CCF) (Eq.(7)) is used to measure the variation of similarity between two signals with time delay and is widely applied in fields such as signal processing and system analysis. This paper proposes a new composition method. Based on the calculation of the signal energy correlation within the time-shifted sliding window by CCF, the statistical average suppression of noise power and the phase alignment enhancement of fault impulse components are achieved, thereby improving the physical interpretability of the edge connection relationship. It is specifically manifested in the following two aspects.

$$CCF_{xy}(\tau) = R_{xy}(\tau) = \int_{-\infty}^{\infty} x(t)y(t+\tau)dt \tag{7}$$

1. The CCF suppresses random noise through the product integration between signals. As shown in Eq.(8), when the signal is in a noisy environment, the noise is usually random and independent of the signal. During the cross-correlation summation process, the CCF values of the noise terms $n_i^p(t)$ and $n_i^q(t)$ tend to be zero, as shown in the Eq.(9). And the cross terms of the signal and noise disappear, which means $R_{x_i^p n_i^q}(\tau) = 0$ and $R_{x_i^q n_i^p}(\tau)$ =0, while the true signal component $R_{x_i^p x_i^q}(\tau)$ is retained. Thereby highlighting the true correlation between the signals.

$$R_{x'^p_i x'^q_i}(\tau) = \int_{i=1}^{l} x'^p_i(t)x'^q_i(t+\tau)\,dt = \int_{i=1}^{l}\left[x_i^p(t) + n_i^p(t)\right]\left[x_i^q(t+\tau) + n_i^q(t+\tau)\right]dt = R_{x_i^p x_i^q}(\tau) + R_{x_i^p n_i^q}(\tau) + R_{x_i^q n_i^p}(\tau) + R_{n_i^p n_i^q}(\tau) \tag{8}$$

$$R_{n_i^p n_i^q}(\tau) = \int_{i=1}^{l} n_i^p(t) \cdot n_i^q(t+\tau) \approx 0 \tag{9}$$

2. Phase Sensitivity and Fault Feature Matching. Rotating machinery faults often generate periodic impacts. However, due to differences in sensor placement or signal propagation paths, signals from different channels may exhibit a fixed phase shift. ED and CS are both similarity metrics evaluated at a fixed time shift, making them sensitive to phase variations. Even if two waveforms are highly similar, the ED can be inflated due to misalignment, and CS becomes inaccurate because the inner product is affected by phase rotation. Consequently, neither metric can reflect the true similarity between signals when a phase offset exists. In contrast, The CCF can accurately identify the optimal time shift that aligns the two signals by evaluating their similarity at different lags, and it assesses their similarity after alignment, thereby effectively eliminating the influence of phase offset and providing a true measure of similarity between the two signals.

The process of constructing the adjacency matrix based on the CCF is shown in Fig. 4, taking the signal samples of channels p and q as an example, channel p contains sample set $\boldsymbol{x^p} = \{x_1^p, x_2^p \ldots x_m^p\}$, and channel q contains sample set $\boldsymbol{x^q} =$

$\{x_1^q, x_2^q \ldots x_n^q\}$. First, calculate the CCF between all sample pairs ($m \times n$) of the two channels. The CCF of the two samples x_m^p and x_n^q is $R_{pq}(m,n,\tau)$, and its peak value is as shown in Eq.(10):

$$R_{m,n}^{max} = max_\tau R_{pq}(m,n,\tau) \quad (10)$$

Subsequently, the top k maximum values are filtered from the peak set through the KNN algorithm, and the corresponding sample pairs form the following set：

$$\varepsilon_{pq} = \{(m^*, n^*) | R_{m^*,n^*}^{max} \in KNN - top_k(R_{pq}) \quad (11)$$

Finally, the elements of the adjacency matrix $A_{(m,p),(j,q)}$as follows:

$$A_{(m,p),(j,q)} = \begin{cases} 1, if\,(m,q) \in \varepsilon_{pq} \\ 0, otherwise \end{cases} \quad (12)$$

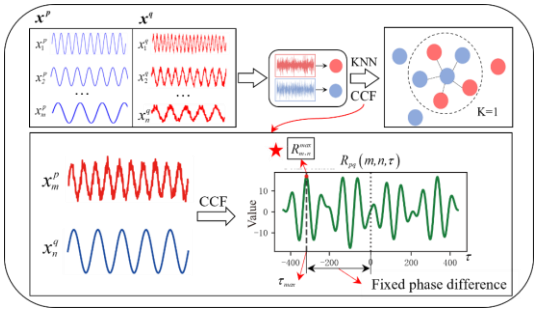

qiqure 4. Constructing multi-channel graph structures based on CCF.

After constructing the graph structure based on CCF, the graph convolutional network is used to further fuse multi-channel features. The graph convolution process is shown in Eq.(14). $\widetilde{\boldsymbol{A}}$ is the adjacency matrix with self-loops, $\widetilde{D}$ is the degree matrix, σ is the activation function, $\boldsymbol{W}^{(l)}$ is the weight matrix, $[\boldsymbol{h}_p^l, \boldsymbol{h}_q^l, \ldots, \boldsymbol{h}_s^l]$ represents the feature matrix composed of multi-channel signals (p, q...s), and $\boldsymbol{H}^{(l+1)}$ represents the aggregated features, which integrate the features of multi-channel signals and are used for downstream classification tasks.

$$\boldsymbol{H}^{(l+1)} = \sigma\left(\widetilde{D}^{-\frac{1}{2}}\widetilde{\boldsymbol{A}}\widetilde{D}^{\frac{1}{2}}[\boldsymbol{h}_p^l, \boldsymbol{h}_q^l, \ldots, \boldsymbol{h}_s^l]\boldsymbol{W}^{(l)}\right) \quad (12)$$

After systematically elaborating the theoretical framework and method design of the improvement strategy of ECGCN, in order to further verify the performance advantages of this model in complex representation learning, the following content will conduct multi-dimensional empirical research. The superiority and effectiveness of ECGCN in the process of intelligent fault diagnosis are proved through specific experiments.

3. Test

3.1. Experiment preparation

3.1.1. Dataset

In this paper, two public bearing datasets are adopted to verify the proposed method. Dataset I is the bearing vibration dataset provided by Southeast University; Dataset II is a bearing dataset provided by Huazhong University of Science and Technology.

1. Dataset I: Bearing vibration dataset of southeast university (SEU)

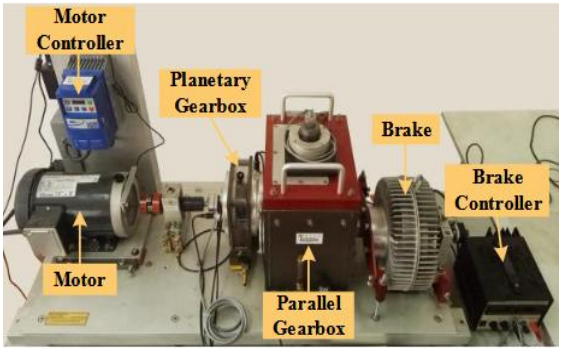

Figure 5. Test rig of SEU bearing dataset.

The SEU bearing dataset was collected from the Drive System Dynamic Simulator. It was collected under two different working conditions with the rotational speed system load set at 20HZ-0V or 30HZ-2V, and the sampling frequency was 5120HZ. The different fault types of bearings are detailed in Table 1. This dataset contains four bearing failure states and one health state. The fault states of the bearings are as follows: cracks appear on the rolling elements, cracks appear on the inner race, cracks appear on the outer race, and cracks appear on both the inner and outer race. In this paper, the data of four types of faulty bearings and healthy bearings under a load condition of 20Hz-0V are adopted as experimental samples. Each type of bearing vibration data contains three channel signals, namely X, Y, and Z, corresponding respectively to the axial, radial horizontal, and radial vertical directions. The X-direction along the bearing axis reflects the axial load and preload state. The Y direction is horizontal radial and sensitive to radial clearance and imbalance. The Z direction is vertical and radial, also reflecting radial loads. Due to the influence of gravity, its characteristics are different from those of the Y direction. Multi-directional collaborative collection can comprehensively capture the vibration characteristics of bearings, which is conducive to improving the accuracy of fault diagnosis. Fig. 6 and Fig. 7 respectively show the time-domain and frequency-

domain graphs of the four types of faulty bearings in the SEU bearing dataset.

Table 1. SEU bearing vibration dataset.

Condition of Loading	Sample Frequency	Fault Type	Channel Acquisition
20Hz-0V、30Hz-2V	5120HZ	Normal Inner race fault (IF) Outer race fault (OF) Ball fault (BF) Comb fault (CF)	X, Y, Z

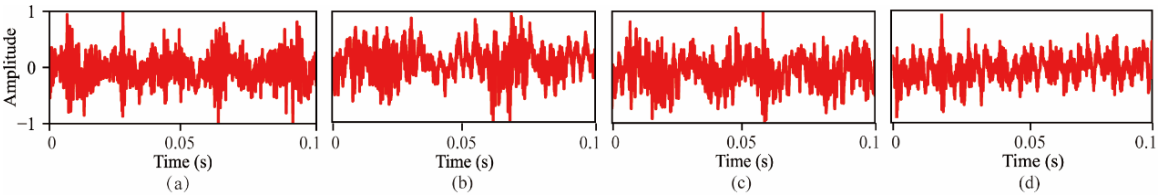

Figure 6. Time-domain graphs (noise-free) of different fault types in the SEU bearing dataset.(a) IF (b) OF (c) BF (d) CF.

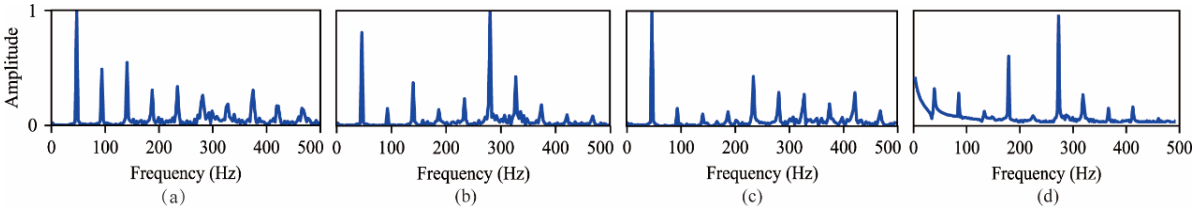

Figure 7. Frequency-domain graphs (noise-free) of different fault types in the SEU bearing dataset.(a) IF (b) OF (c) BF (d) CF.

2. Dataset II: bearing vibration dataset of Huazhong university of science and technology (HUST) [34].

The HUST dataset collected bearing vibration signals in different states under 11 rotational speed conditions (10 constant rotational speeds and 1 time-varying rotational speed), with a sampling frequency of 25.6KHz. The different fault types of the bearings are detailed in Table 2.

This dataset contains 8 bearing failure states and 1 health state. The bearing failure states respectively include severe damage to the inner race, outer race, rolling elements and compound faults. In this paper, the data of four types of faulty bearings in a severely damaged state and bearings in a healthy state under the condition of 20Hz rotational speed are adopted as experimental data samples. Each type of bearing vibration data contains three channel signals, namely X, Y, and Z, corresponding respectively to the axial, radial horizontal, and radial vertical directions. Fig. 9 and Fig. 10 respectively show the time-domain and frequency-domain graphs of the four types of faulty bearings in the HUST bearing dataset.

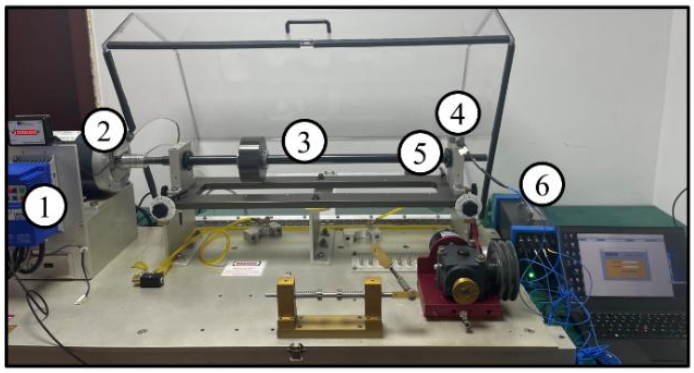

1: Speed control, 2:Motor, 3: Shaft, 4: Acceleration sensor, 5: Bearing, 6: Data acquisition board

Figure 8. Test rig of HUST bearing dataset.

Table 2. HUST bearing vibration dataset.

Condition of Loading	Sample Frequency	Fault Type	Channel Acquisition
20Hz；25Hz；30Hz；35Hz；40Hz；60Hz；65Hz；70Hz；75Hz；80Hz；0-40-0Hz	25.6KHz	Normal Inner-race fault（IF）（Severe、Medium） Outer-race fault(OF) （Severe、Medium） Ball fault(BF) （Severe、Medium） Comb fault(CF) （Severe、Medium）	X,Y,Z

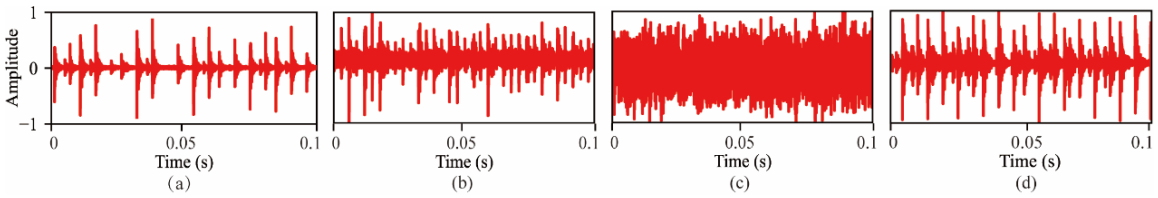

Figure 9. Time-domain graphs (noise-free) of different fault types in the HUST bearing dataset.(a) IF (b) OF (c) BF (d) CF.

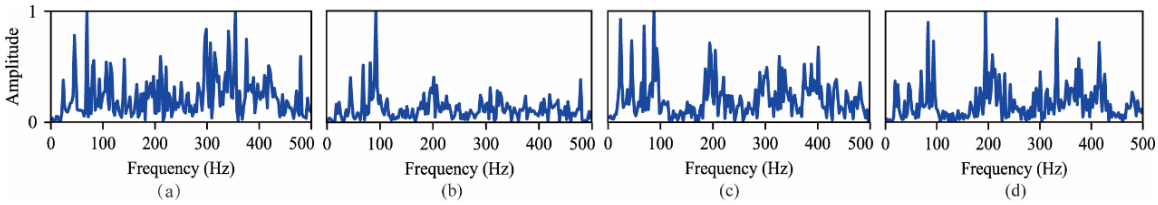

Figure 10. Frequency-domain graphs (noise-free) OF different fault types in the HUST bearing dataset. (a) IF (b) OF (c) BF (d) CF.

In actual industrial scenarios, the collected data usually contains various types of background noise. However, the above-mentioned experimental data set was collected in a relatively ideal laboratory environment, and the noise interference it contains is limited. To more effectively verify the anti-noise performance of the proposed model under near-real working conditions, this paper adopts the method of adding Gaussian white noise with different Signal-to-Noise ratios (SNR) to conduct noise enhancement processing on the existing data set, in order to simulate the complex noise interference situation in the actual industrial environment. Among them, the lower the signal-to-noise ratio, the greater the noise intensity and the higher the degree of data contamination. The specific calculation method for adding Gaussian white noise is shown in the Eq.(15).

$$x_{noisy}(t) = x(t) + n(t) \tag{13}$$

Among them: x(t) is the original signal, n(t) is Gaussian white noise, with a mean of 0 and a variance of σ^2, and x_{noisy} is the signal after adding noise.

The calculation for the SNR is is shown in the Eq.(16). $\sigma[x^2(t)]$ represents the variance of the original signal, and $\sigma[n^2(t)]$ represents the variance of the noise. The smaller the SNR, the greater the noise intensity and the higher the degree of data contamination. By adjusting the value of SNR, the intensity of the added noise can be controlled, thereby simulating the data characteristics under different noise environments.

$$SNR = 10log_{10}\left(\frac{\sigma[x^2(t)]}{\sigma[n^2(t)]}\right) \tag{14}$$

3.1.2. Sample selection and evaluation indicators

(1) Sample selection

Vibration signals contain rich fault characteristics. A reasonable sample length is crucial for effective feature extraction, and it is necessary to take into account signal integrity, computational efficiency and model requirements. This paper choose 1024 points sampling length, according to the following:

1. The frequency resolution: the length under the common sampling rate can meet dozens to hundreds of Hertz low-frequency fault components analysis requirements, to ensure that features extracted effectively.
2. Computational efficiency: in full cycle of information at the same time, control calculation burden, to adapt to the depth of the model input.
3. Enhance flexibility: easy to use in the form of sliding window, overlap sampling and data, model generalization ability.
4. Each sensor selected 100 samples, in accordance with the ratio 6:2:2 divided into training set, validation set and test set, in order to ensure model training, tuning fully effective and independent evaluation.

(2) Evaluation index selection

As shown in Table 3, using Accuracy (ACC), Precision (Pre), Recall, (Rec) and F1 score (F1) performance evaluation of bearing fault diagnosis model for classification.

1. ACC: It reflects the overall classification accuracy rate and is suitable for scenarios with balanced categories.
2. Pre: measure of forecasting accuracy, reduce the false alarm.

3. Rec: measure of the ability to identify the real positive cases in fault diagnosis is very important.
4. F1: comprehensive Pre and the harmonic average of Rec, unbalanced situation is suitable for processing category.
5. The multi-target combination can be evaluation model from various angles, to provide more comprehensive basis for optimization.

Table 3. Model evaluation index.

Metric	Expression
Accuracy	$\frac{tp+tn}{tp+fp+tn+fn}$
Precision	$\frac{tp}{tp+fp}$
Recall	$\frac{tp}{tp+fn}$
F1-score	$\frac{2 \times \text{Precision} \times \text{Recall}}{\text{Precision} + \text{Recall}}$

3.1.3. Training parameters

As shown in Table 4, ECGCN is trained using the Adam optimizer and the cross-entropy loss function. Meanwhile, to prevent overfitting, L1 regularization is added to the loss function. The training period is set to 1000, the learning rate to 0.01, and the patience value to 20. (When the accuracy of the model tends to stabilize, stop training when the accuracy of the model has not improved after 20 rounds of training.)

Table 4. ECGCN training parameters.

Optimizer	Loss function	Regularization	Number of epochs	Learning Rate	Patience
Adam	Cross entropy	L1	1000	0.01	20

3.2. Ablation experiment for improving the effectiveness of the strategy

This section aims to systematically evaluate the optimization effect of each improvement strategy on the anti-noise performance of the model based on different SNRs. Experiments are conducted based on the SEU bearing dataset, and the experiments are divided into two modules:

1. Focus on improving the effect of envelope activation in the convolutional layer, quantify its performance gain under different SNRS through ablation experiments, and simultaneously analyze its interpretability in suppressing noise and enhancing feature representation.
2. A comparative analysis is conducted on the graph structure construction methods, with a focus on verifying the superiority of the composition strategy based on the CCF over the composition methods based on ED and CS, revealing its unique advantages in feature correlation modeling.

3.2.1. Verification and Analysis of the Superiority of envelope activation

To explore the influence of the envelope activation mechanism on the anti-noise performance of the model, this study conducted experiments using the strict control variable method. By constructing a control experiment system, the experimental group model containing the envelope activation module and the control group model with the module removed were trained respectively. Under the multi-gradient SNR conditions ranging from -15dB to 15dB, the classification ACC of the two types of models were compared and analyzed horizontally to evaluate the effect of the envelope activation mechanism. Meanwhile, combined with the T-SNE visualization technology, from the dimension of the spatial distribution of data features, the shaping effect of envelope activation on the classification decision boundary is analyzed to provide an interpretable basis for the mechanism of improving the anti-noise performance of the model.

Fig. 11 shows the classification ACC of the models with and without envelope activation modules under different SNR conditions. In an extremely strong noise environment (SNR=-15dB, -10dB), the control group models without envelope activation modules exhibit significant performance degradation, with classification ACC dropping to 58.67% and 60.33% respectively, demonstrating obvious noise sensitivity. In sharp contrast, the experimental group model with the envelope activation module demonstrated outstanding anti-noise robustness, maintaining a high classification ACC of over 90% under the same harsh conditions. This fully verified the significant improvement effect of the envelope activation mechanism on model performance in extreme noise scenarios.

Fig. 12 shows the T-SNE visualization comparison of the model classification results with and without envelope activation modules under different SNR conditions. The experimental results show that for the model without the envelope activation module under each SNR condition, its T-SNE graph presents the characteristics of discrete distribution of data points and blurred clustering boundaries, reflecting that

the model is difficult to effectively distinguish different types of data, resulting in poor classification performance. Compared with the T-SNE diagrams generated by the models with envelope activation modules, the data points of various categories are closely clustered, the clustering structure is clear and distinguishable, and the separation degree between classes is significantly improved. This intuitively confirms that the envelope activation module can effectively enhance the feature expression ability of the model and significantly improve the classification effect.

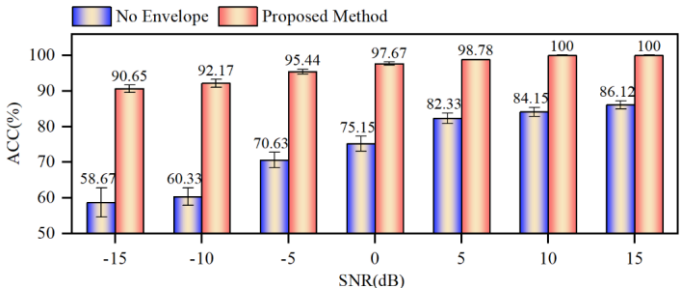

Figure 11. Model classification ACC with and without envelope activation modules (different SNRs).

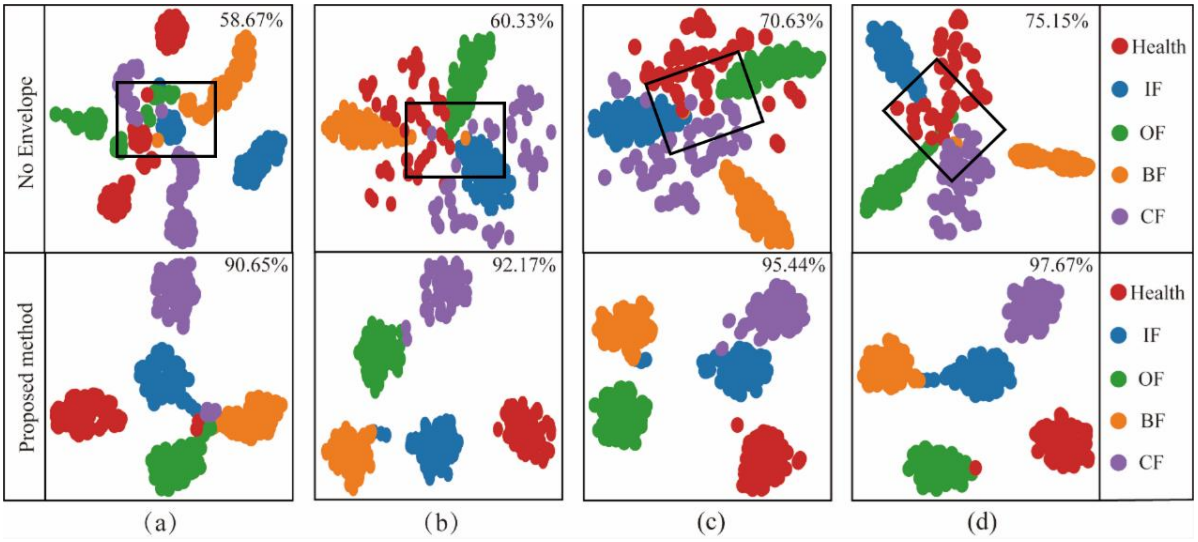

Figure 12. Visualization of the impact of envelope activation on model classification. (a) ~ (d) represent the classification T-SNE of the non-envelope activation (upper) and the complete model (lower) with SNR of -15dB, -10dB, -5dB, and 0dB, respectively.

To explore the interpretability of the envelope activation module in noise suppression and the improvement of feature representation capabilities, the output features of the convolutional layer were subjected to envelope activation processing. The activated signal is shown inFig. 13: In the time domain, the signal features after envelope activation processing show more prominent periodicity compared to the original features. This periodic feature is precisely the key characterization of the fault signal. Envelope activation effectively enhances the weak periodic components submerged in the noise. By significantly amplifying the fault characteristics, it suppresses the background noise and thereby improves the anti-noise performance of the model. In the frequency domain, the noise energy is uniformly distributed in the frequency domain. Envelope activation can enhance the low-frequency modulation components and suppress the noise components. The characteristic frequencies in the original signal that are submerged by wideband noise are transformed into energy-concentrated spectral peaks after envelope activation. Essentially, this process is to focus the dispersed signal energy in the wideband noise background to the characteristic frequency points through energy redistribution in the frequency domain. So as to achieve the enhancement of robustness characteristics.

In conclusion, the envelope feature can highlight the abnormal amplitude changes in the signal, making the features related to the fault more obvious. It is helpful to extract the fault feature information from the complex noise background, thereby improving the accuracy and reliability of fault diagnosis.

Based on the above multi-dimensional data analysis and comprehensive consideration, the unique advantages and irreplaceability of each improvement strategy of ECGCN in the noisy environment were verified respectively, and a deep learning framework with noise-resistant robustness was jointly constructed.

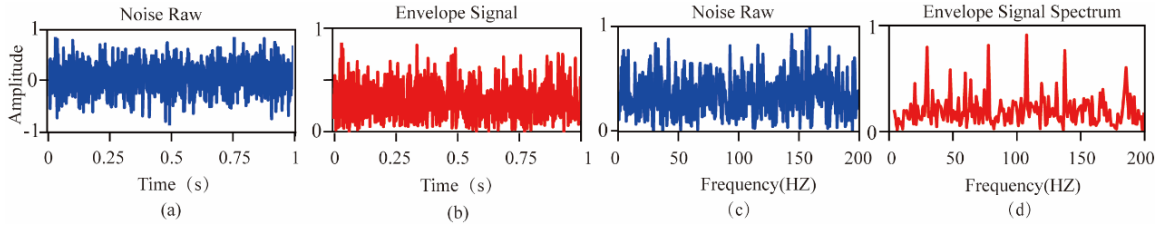

Figure 13. The effect of envelope activation on strong noise signals (SNR=-10). (a) Convolutional layer time-domain signal (b) Signal after envelope activation (c) Convolutional layer frequency-domain signal (d) Frequency-domain signal after envelope activation.

3.2.2. Verification and Analysis of the Superiority of the CCF

In graph convolutional neural networks, the adjacency matrix $\widehat{\boldsymbol{A}}$, as the core computing unit, directly affects the feature propagation effect. Therefore, the graph structure construction method is very crucial. During the process of multi-channel vibration signal acquisition, due to the influence of mechanical structure characteristics, phase offset is inevitable in the process of collecting multi-channel vibration signals, and this offset may cause coupling interference to the fault characteristics. The CCF, as the similarity measure of the time difference τ parameter (τ represents the time difference of signal alignment), when constructing the edge connection model, through the introduced time-shift compensation mechanism, can effectively decouple the influence of phase offset on feature representation. This study conducts experiments based on the SEU bearing dataset to systematically analyze the influence of the time-shift parameter τ on the CCF value and the constructed graph edge connection topology. By comparing the two modes of $\tau = 0$ (without phase compensation) and $\tau \neq 0$ (with phase compensation), the role of τ in a noisy environment is verified.

The time-shift parameter scanning experimental results of the dual-channel signal samples are shown in Table 5 (under different SNR conditions), and the classification ACC of the model is shown in Fig. 14. It can be seen from the experimental results that the change of the CCF response shows significant sensitivity. This sensitivity is conducted to the graph topology construction process and ultimately affects the classification effect of the model. Therefore, in the experiment, the one corresponding to the maximum value of the CCF is selected to compensate for the phase deviation caused during the process of collecting multi-channel signals.

Table 5. The influence of τ on the value of the cross-correlation function.

τ(s) / Values(%) / SNR(dB)	0	0.02	0.04	0.06	0.08	0.1
-15	38.63	-57.32	-149.57	-41.36	-31.84	-8.48
-10	26.02	5.4	-2.06	7.54	-1.07	2.85
-5	6.74	15.57	-11.82	-9.82	-9.12	-20.05
0	-12.64	-3.22	1.7	-10.55	5.89	-5.21
5	-7.5	-4.05	-3.25	-10.97	4.34	-7.51
10	-11.29	-3.13	-2.89	-5.77	1.90	-5.14
15	-8.82	0.06	-2.67	-5.99	4.50	-3.59

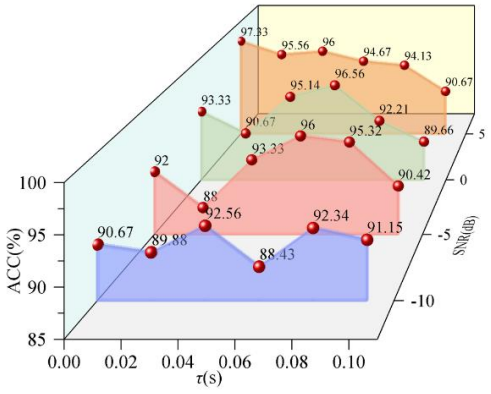

Figure 14. The influence of on the classification effect of ECGCN (Different SNRs).

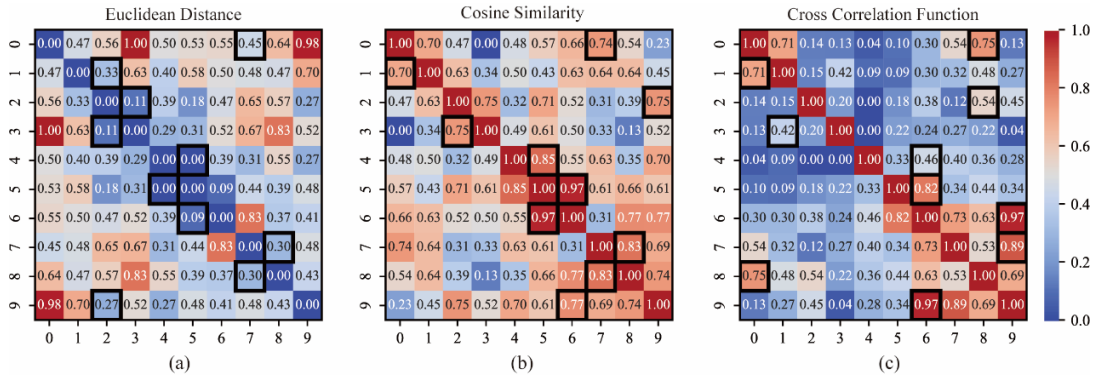

Figure 15. Heat maps of the strength of the relationship between nodes described by different composition methods (After global normalization, ED is negatively correlated with the sign correlation, while CS and CCF are positively correlated with the signal correlation).(a) Based on Euclidean distance (b) Based on cosine similarity (c) Based on cross-correlation function.

After completing the quantitative analysis of the influence of τ on the CCF and its model, the focus is on exploring the influence of different graph construction methods on the classification performance. By comparing three methods: ED, CS, and CCF, a heat map matrix of the correlation strength between signals was constructed based on ten samples of strong noise signals. The visualization results shown in Fig. 15 indicate that the three methods present significantly differentiated results when characterizing signal correlations.

As shown in Fig. 16, under each SNR condition, the classification F1-score of the models constructed based on the ED and CS mapping methods are both lower than those based on the CCF mapping method, and the classification effect of their models is poor. The graph structure based on the essential correlation of signals provides a feature expression space with stronger noise resistance for the subsequent graph convolution, enabling the model to have a higher F1 index under the same noise conditions and verifying the dual advantages of the cross-correlation function in noise suppression and feature preservation.

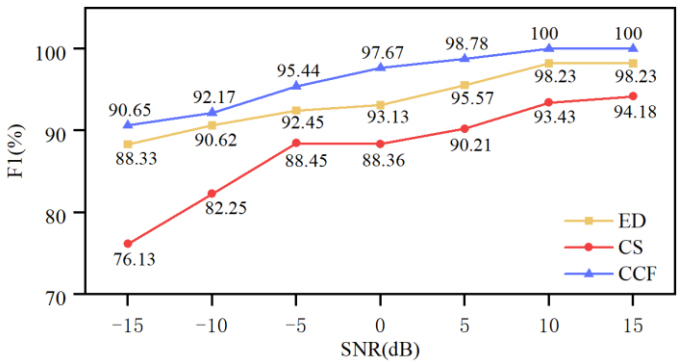

Figure 16. Model classification F1 when composing with different methods.

3.3. Model diagnostic performance comparison experiment

To verify the superiority of ECGCN, different deep learning models were selected. Comparative experiments on the classification effects of the models were conducted based on the SEU dataset and the HUST dataset respectively under noise-free conditions and different SNR conditions. The selected comparison models are GCN, GAT, Graph SAGE, GIN, HO-GCN ,1D CNN and LSTM, and the model inputs are all multi-channel vibration signals. The model parameters are show in Table 6.

3.3.1. Comparative experiments based on the SEU dataset

Firstly, the SEU multi-channel vibration signals were input into each comparison model under noise-free conditions. The classification results of each model are shown in Table 7. The results show that under the noise-free condition of the SEU dataset, all classification indicators of the ECGCN model can reach 100%, and Graph neural networks such as GCN, GAT and Graph SAGE all maintain high classification accuracy. However, each evaluation index of the 1D CNN and LSTM models showed significant attenuation.

In order to verify the superiority of the anti-noise performance of ECGCN, multi-channel vibration signals under different SNR conditions were input into each graph neural network model, and the classification ACC is shown in Table 8 and Fig. 17. The results show that in terms of training efficiency, although CEGCN takes a relatively long time (202.54s), its classification accuracy in a noisy environment is significantly better than that of graph neural network models such as GCN

and GAT. Even under strong noise interference (SNR=-15), CEGCN can still maintain a classification accuracy of over 90%.

The classification confusion matrices of each model under SNR=-15 are shown in Fig. 18. In the confusion matrices of the comparison models: GraphSAGE, GCN, GAT, HO-GCN and GIN, there are generally more misclassified samples, indicating that the discriminative ability of the models significantly decreases under the interference of strong noise. The confusion matrix of the CEGCN model demonstrates high diagnostic accuracy and anti-noise robustness. The various samples are basically concentrated along the diagonal, with fewer misjudgments.

Table 6. Compare the parameter Settings of the model.

Model	Hyper-parameter	Trainable parameters
ECGCN	Kernel Size=16; Channel=10; Drop=0.5	Convolutional layer①：（1024，512） Convolutional layer②：（512，256）
GCN [35]	Drop=0.5	Convolutional layer①：（1024，512） Convolutional layer②：（512，256）
GAT [36]	Head=4; Drop=0.5	Convolutional layer①：（1024，512） Convolutional layer②：（512，256）
Graph SAGE [37]	Drop=0.5	Convolutional layer①：（1024，512） Convolutional layer②：（512，256）
GIN [38]	Aggregator type=Sum; Drop=0.5	Convolutional layer①：（1024，512） Convolutional layer②：（512，256）
HO-GCN [39]	Maximum neighborhood order=3; Drop=0.5	Convolutional layer①：（1024，512） Convolutional layer②：（512，256）
1D CNN [31]	Kernel Size=16; Channel=10	Convolutional layer（1024，256）
LSTM [40]	Sequence Length=1024; Hidden Units=512	Hidden layer（1024，512）

Table 7. Classification effects of various comparison models under noise-free conditions (SEU dataset).

Model / Values(%)	ECGCN	GCN	GAT	Graph SAGE	GIN	HO-GCN	1D CNN	LSTM
ACC	100	89.67	90.33	87.22	100	100	20.00	20.00
Pre	100	88.94	89.74	73.62	100	100	4.00	4.00
Rec	100	89.67	90.33	87.22	100	100	20.00	20.00
F1	100	88.65	90.15	79.19	100	100	6.76	6.76

Table 8. Compare the classification accuracy and training time of the models under different SNRs (SEU dataset).

Model		GCN	GAT	GIN	GraphSAGE	HO-GCN	CEGCN
SNR	-15	56.67±6.67	60.12±3.19	69.55±4.22	49.16±3.36	78.67±4.16	90.65
	-10	60.15±3.21	63.45±2.24	76.53±4.3	51.76±1.76	84.80±0.72	92.17±0.92
	-5	71.33±1.45	73.43±0.44	82.93±1.76	55.49±1.33	87.47±0.67	95.44±0.67
	0	75.86±2.14	80.16±1.05	86.67±1.31	62.16±1.15	93.73±0.77	97.67±0.28
	5	77.16±1.12	84.33±1.43	91.07±1.25	71.33±0.56	94.93±1.22	98.78±0.20
	10	82.46±1.45	86.25±1.67	93.20±1.05	73.34±0.96	97.20±0.18	100±0.00
	15	85.62±1.02	90.11±0.68	96.67±0.43	85.67±0.44	98.12±014	100±0.00
Time(s)		26.34s	28.25s	37.65s	36.18s	53.46s	202.54s

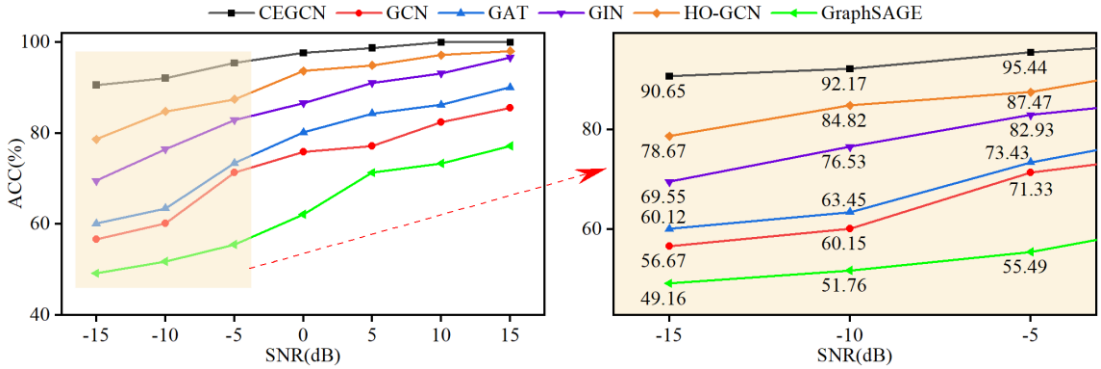

Figure 17. Comparison of model classification ACC under different SNRs. The right figure shows the enlarged shaded part of the left figure (SEU dataset).

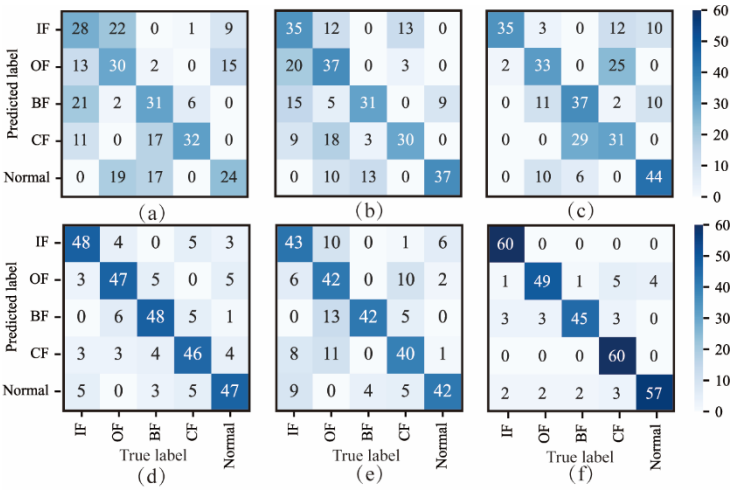

Figure 18. Confusion matrix for classification of different models under SNR=-15 (SEU dataset)

（a）GraphSAGE（b）GCN（c）GAT（d）HO-GCN（e）GIN（f）CEGCN.

3.3.2. Comparative experiments based on the HUST dataset

To verify the generalization performance of the model, noise-free comparative experiments were conducted on the HUST dataset, and the results are shown in Table 9. The experimental conclusion is consistent with the results of the SEU dataset: Graph neural network models (such as GCN, GAT, GraphSAGE, etc.) can effectively extract fault features from multi-channel signals and have a relatively high classification accuracy. However, 1D CNN and LSTM are not sensitive to multi-channel signals and have poor classification performance. This indicates that there are significant differences among different models in the feature learning and classification capabilities of multi-channel vibration signals.

To verify the generalization ability of the noise resistance performance of CEGCN, further comparative experiments were conducted on the HUST bearing dataset. The results are shown in Table 10 and Fig. 19. Experiments show that under different SNRs, although the training time of CEGCN is relatively long (225.46s), it still achieves a high classification accuracy on the HUST dataset and outperforms other comparison models.

The classification confusion matrices of each model under SNR=-15 are shown in Fig. 20. The colors of the confusion matrix of CEGCN are most concentrated on the diagonal, while those of other models are much more dispersed. It is indicated that the classification effect of CEGCN is significantly better than that of other graph neural network models such as GraphSAGE and GCN even under strong noise.

Table 9. ssification effects of various comparison models under noise-free conditions (HUST dataset).

Model / Values(%)	ECGCN	GCN	GAT	Graph SAGE	GIN	HO-GCN	1D CNN	LSTM
ACC	100	92.00	94.67	91.11	100	100	28.67	19.67
Pre	100	93.33	95.12	91.67	100	100	19.46	3.96
Rec	100	92.00	94.67	91.11	100	100	28.67	19.67
F1	100	90.15	95.48	90.11	100	100	19.03	6.59

Table 10. Compare the classification accuracy and training time of the models under different SNRs. (HUST dataset)

Model		GCN	GAT	GIN	GraphSAGE	HO-GCN	CEGCN
SNR	-15	56.67±7.25	60.12±7.15	70.55±3.23	51.35±1.33	69.67±5.12	88±1.36
	-10	67.33±7.03	70.34±4.63	72.14±6.38	58.15±0.92	80.40±4.14	89.33±1.02
	-5	70.17±6.14	75.56±2.03	73.88±4.76	62.44±1.05	82.16±3.55	92.11±0.88
	0	72.67±3.12	79.33±2.41	77.62±4.31	71.13±1.33	82.33±3.88	96.34±0.67
	5	80.15±3.05	81.24±1.09	80.58±2.84	79.67±0.88	85.67±2.18	98.67±0.00
	10	83.33±2.24	88.67±1.03	86.23±2.09	80.15±0.43	88.08±0.43	98.67±0.00
	15	86.67±2.26	90.17±0.88	93.72±1.02	83.33±1.02	95.12±0.14	100±0.00
Time(s)		30.12s	32.33s	42.36s	44.25s	62.09s	225.46s

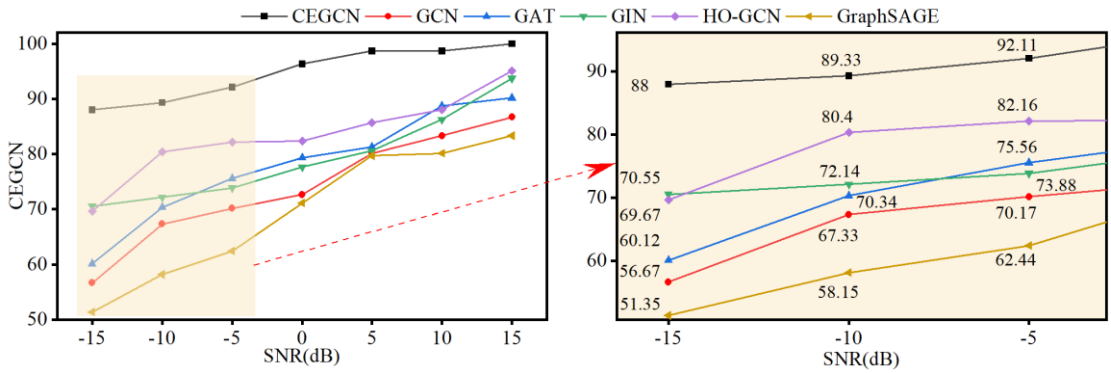

Figure 19. Comparison of model classification ACC under different SNRs. The right figure shows the enlarged shaded part of the left figure (HUST dataset).

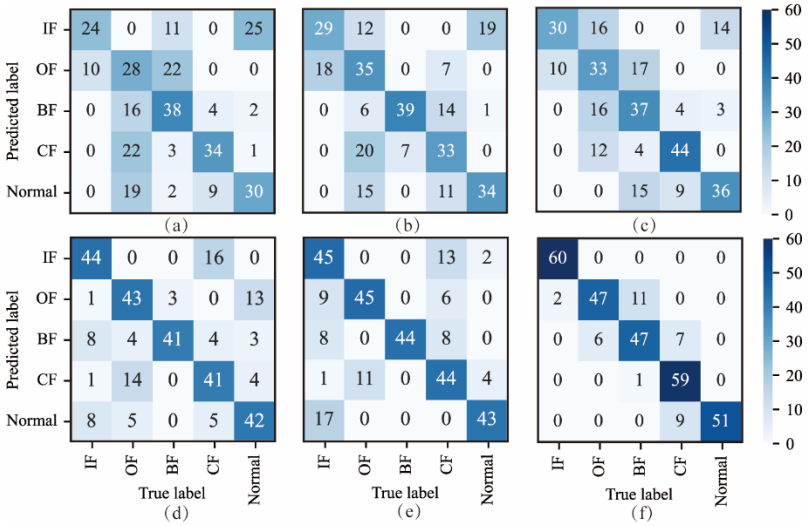

Figure 20. Confusion matrix for classification of different models under SNR=-15. (HUST dataset)
（a）GraphSAGE（b）GCN（c）GAT（d）HO-GCN（e）GIN（f）CEGCN.

Combining the experimental results on the SEU and HUST datasets, CEGCN demonstrates excellent classification performance in various noise environments, fully demonstrating that this model has good generalization ability and noise resistance robustness under complex noise conditions. Its anti-noise advantage stems from a unique cascaded processing architecture: on the one hand, the improved convolutional layer suppresses wideband noise through local feature extraction and envelope activation; On the other hand, in the integration operation of CCF, phase interference is eliminated by the selection of positive and negative random noise and time-shift parameters. Finally, the multi-channel features with enhanced noise resistance are input into the graph convolutional network to enhance the feature representation. This collaborative mechanism of noise filtering and feature enhancement enables CEGCN to maintain the optimal classification performance in strong noise scenarios.

3.4. Further Discussion

3.4.1. K value optimization experiment

In the process of constructing the multi-channel signal graph structure based on CCF, we adopt the KNN algorithm to establish the connections between multi-channel signal samples. Among them, the composition parameter K value directly determines the tightness of the topological connection of multi-channel signals, and thus has an important impact on the subsequent multi-channel signal fusion effect. This subsection systematically explores the impact of the K value on the classification performance and memory occupancy of the CEGCN model based on the HUST dataset.

Fig. 21 shows the classification effect of CEGCN under SNR=0, and Table 11 presents the size of the model's running memory. It can be seen that as the K value increases, the classification performance of CEGCN (ACC, Pre, Rec, F1) generally shows a trend of first rising and then stabilizing. When

K=8, all the indicators of the model tend to converge. Meanwhile, the memory usage of the model increases with the increase of the K value. It is 3.22G when K=8, which is higher than K=3 (1.57G), but much lower than K=12 (4.02G). Taking into account the classification effect and computational cost comprehensively, K=8 achieves the best balance between performance and efficiency, and thus is determined as the optimal parameter.

Table 11. The occupied space of CEGCN operation.

K	3	4	5	8	10	12
Memory(G)	1.57	2.44	2.88	3.22	3.62	4.02

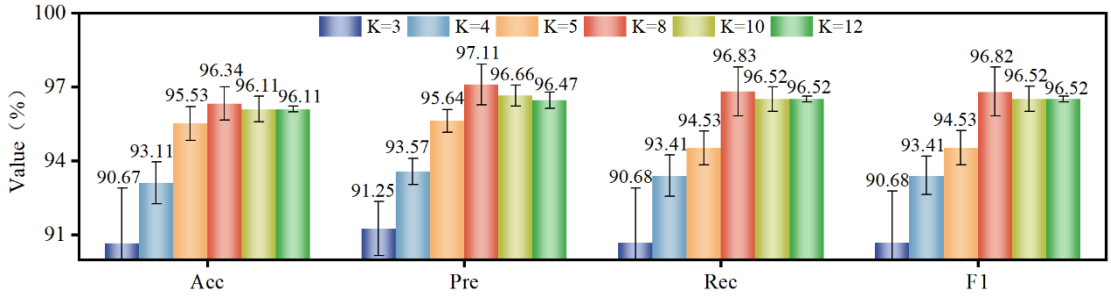

Figure 21. The influence of K value on the classification effect of CEGCN.

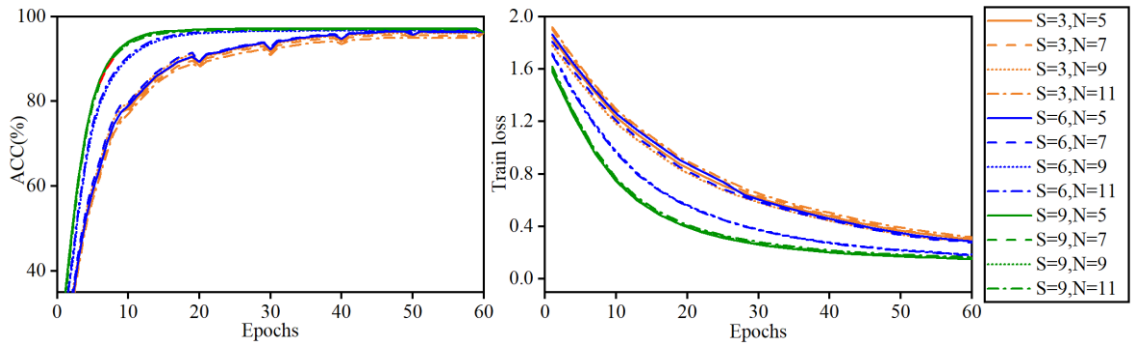

Figure 22. Model training process (S is convolution kernel size, N is the number of convolution kernels).

3.4.2. Optimal selection of independent and parallel convolution kernel parameters

CEGCN conducts preliminary fault feature extraction on multi-channel vibration signals by adopting independent and parallel convolutional layers. Among them, the parameter setting of the convolutional kernel has a key impact on the model convergence process and classification accuracy. This experiment aims to explore the influence law of different combinations of convolution kernel parameters on the performance of the CEGCN model. By training on the HUST dataset under the condition of SNR=0, the results are shown in Fig. 22. Analysis shows that increasing the size of the convolution kernel (such as S=9) can effectively accelerate the convergence speed of the model in the early stage of training, while the change in the number of convolution kernels (N taken as 5, 7, 9, 11) has no significant impact on the model training process. Furthermore, after thorough training, the models under different parameter combinations can all converge to similar final classification accuracy rates, indicating that CEGCN has good stability and robustness under different hyperparameter configurations.

3.4.3. Superiority Verification and Analysis of Multi-channel Models

This study aims to systematically verify the enhancing effect of the multi-channel feature fusion mechanism on the classification performance of the ECGCN model. In the text, the model with single-channel signals as input is defined as the single-channel model, and the model with multi-channel signals as input is defined as the multi-channel model. A comparative experiment was carried out based on the SEU bearing dataset. By comparing the classification performance differences between the single-channel model and the multi-channel model under different SNR conditions, the superiority of the multi-channel model was revealed. In the experiment, the X-axis vibration signal was selected as the input of the single-channel model. By strictly matching parameters such as the sampling

frequency, sample size and signal length (completely consistent with the multi-channel model), the interference of irrelevant variables on the experimental results was effectively eliminated to ensure the reliability of the performance comparison.

The experimental results are shown in Fig.23. When the noise is relatively small (SNR=15, 10), the classification ACC of the single-channel model and the multi-channel model are not much different and can both be maintained above 95%. However, under the condition of strong noise (SNR=-15, -10), the classification ACC of the single-channel model is significantly lower than that of the multi-channel model.

The experimental results show that, based on the improved convolutional layer denoising framework, the multi-channel vibration signals achieve the adaptive fusion of cross-channel features through the Graph Convolutional network (GCN), forming a complementary feature enhancement effect. Compared with the problems such as single feature representation dimension and poor anti-interference ability existing in single-channel signals, multi-channel feature fusion can effectively integrate fault-sensitive features in different directions. Under the extreme noise of SNR=-15dB, the average ACC value can still be as high as 90.65%.

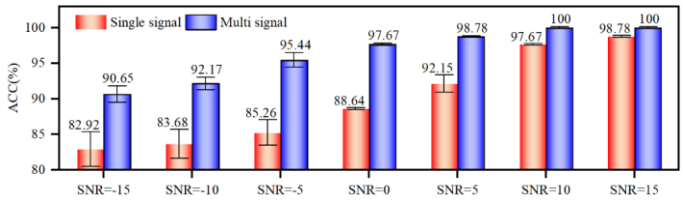

Figure 23. The classification ACC of single-channel models and multi-channel models (Different SNRs).

4. Conclusions and prospects

This paper aims at the challenges of feature extraction and multi-channel signal fusion in a strong noise environment in industrial equipment fault diagnosis, and proposes an improved GNN model based on envelope activation features and cross-correlation function mapping strategy. The model advantages are as follows:

1. A method based on the parallel independent improved one-dimensional convolution architecture is proposed, combined with the envelope activation mechanism to achieve feature extraction of single-channel signals. This architecture design effectively enhances the significance of fault impact features and simultaneously achieves the suppression effect on noise components, providing a high-discrimination feature input basis for subsequent cross-channel feature fusion.
2. A graph structure construction method based on the time-domain cross-correlation function was designed, which effectively overcomes the noise sensitivity in the traditional composition based on Euclidean distance and cosine similarity. This graph structure can effectively represent the inherent feature correlation of multi-channel vibration signals. Combined with the graph convolutional network, the robust fusion of cross-channel features is achieved, significantly improving the signal representation ability.
3. Experiments based on the SEU and HUST public bearing datasets show that the ECGCN model maintains high classification ACC and noise resistance under different SNRs, and its fault identification performance in extreme noise environments is significantly better than that of traditional GNN and deep learning models. Compared with single-channel signals, the multi-channel fusion mechanism can effectively improve the ability of fault feature extraction and the generalization performance of the model.

However, this method still has the following limitations:

1. CEGCN rely on synchronous data acquisition of multi-channel signals of sensor layout and data alignment has certain requirements.
2. The graph construction method based on CCF has high computational complexity, may affect in real time or limited resources deployment efficiency of the scene.
3. Although the present study focused on the bearing fault diagnosis, but this method can be extended to the gear, theoretically rotor and other condition monitoring of rotating machinery system, the future will pass more mechanical datasets verify its generalization performance.

Above all, CEGCN through innovative feature extraction and map building strategy, improve the noise environment of fault diagnosis accuracy and robustness, good engineering application potential. Subsequent work will focus on the deployment and verification in actual industrial scenarios, and further explore the fusion of multimodal signals and the design

of lightweight graph structures to enhance the practicality and adaptability of the model in complex mechanical systems and edge environments.

References

1. Lee J, Wu F, Zhao W, Ghaffari M, Liao L, Siegel D. Prognostics and health management design for rotary machinery systems—reviews, methodology and applications. Mechanical Systems and Signal Processing 2014; 42: 314–334. https://doi.org/10.1016/j.ymssp.2013.06.004.
2. Cheng Y, Lin M, Wu J, Zhu H, Shao X. Intelligent fault diagnosis of rotating machinery based on continuous wavelet transform-local binary convolutional neural network. Knowledge-Based Systems 2021; 216: 106796. https://doi.org/10.1016/j.knosys.2021.106796.
3. Wang J, Du G, Zhu Z, Shen C, He Q. Fault diagnosis of rotating machines based on the EMD manifold. Mechanical Systems and Signal Processing 2020; 135: 106443. https://doi.org/10.1016/j.ymssp.2019.106443.
4. Yang Y, Li Y, Liu X, Feng K. Research on composite impact fault identification algorithm based on improved MLP and single sensor data. 2022 Global Reliability and Prognostics and Health Management (PHM-Yantai), Yantai, China: IEEE; 2022: 1–8. https://doi.org/10.1109/PHM-Yantai55411.2022.9942075.
5. Li Z, Feng-Qi Zhang, Shu-Ting Wan. RBFN based on two levels iteration cluster algorithm and its application in generator fault diagnosis. 2009 International Conference on Machine Learning and Cybernetics, Baoding, China: IEEE; 2009: 1183–1187. https://doi.org/10.1109/ICMLC.2009.5212435.
6. Lu F, Tong Q, Jiang X, Du S, Xu J, Huo J, et al. Envelope spectrum neural network with adaptive domain weight harmonization for intelligent bearing fault diagnosis under cross-machine scenarios. Advanced Engineering Informatics 2024; 62: 102787. https://doi.org/10.1016/j.aei.2024.102787.
7. Li R, Xia T, Luo F, Jiang Y, Chen Z, Xi L. Hybrid physics-embedded recurrent neural networks for fault diagnosis under time-varying conditions based on multivariate proprioceptive signals. Advanced Engineering Informatics 2024; 62: 102851. https://doi.org/10.1016/j.aei.2024.102851.
8. Zhang Z, Wu L. Graph neural network-based bearing fault diagnosis using granger causality test. Expert Systems with Applications 2024; 242: 122827. https://doi.org/10.1016/j.eswa.2023.122827.
9. Zhu Z, Lei Y, Qi G, Chai Y, Mazur N, An Y, et al. A review of the application of deep learning in intelligent fault diagnosis of rotating machinery. Measurement 2023; 206: 112346. https://doi.org/10.1016/j.measurement.2022.112346.
10. Wang C, Jie H, Yang J, Gao T, Zhao Z, Chang Y, et al. A multi-source domain feature-decision dual fusion adversarial transfer network for cross-domain anti-noise mechanical fault diagnosis in sustainable city. Information Fusion 2025; 115: 102739. https://doi.org/10.1016/j.inffus.2024.102739.
11. Wang C, Liu X, Yang J, Jie H, Gao T, Zhao Z. Addressing unknown faults diagnosis of transport ship propellers system based on adaptive evolutionary reconstruction metric network. Advanced Engineering Informatics 2025; 65: 103287. https://doi.org/10.1016/j.aei.2025.103287.
12. Wang C, Jie H, Yang J, Zhao Z, Gao R, Suganthan PN. A virtual domain-driven semi-supervised hyperbolic metric network with domain-class adversarial decoupling for aircraft engine intershaft bearings fault diagnosis. IEEE Trans Syst Man Cybern, Syst 2025; 55: 7950–7963. https://doi.org/10.1109/TSMC.2025.3598790.
13. Wang C, Wu Y, Yang J, Yang B. Continuous evolution learning: A lightweight expansion-based continuous learning method for train transmission systems fault diagnosis. IEEE Transactions on Industrial Informatics 2025; 21: 8270–8281. https://doi.org/10.1109/TII.2025.3588608.
14. Zhu L, Wang J, Chen M, Liu L. Fusion-driven fault diagnosis based on adaptive tuning feature mode decomposition and synergy graph enhanced transformer for bearings under noisy conditions. Expert Systems with Applications 2025; 260: 125441. https://doi.org/10.1016/j.eswa.2024.125441.
15. Kiranyaz S, Avci O, Abdeljaber O, Ince T, Gabbouj M, Inman DJ. 1D convolutional neural networks and applications: A survey. Mechanical Systems and Signal Processing 2021; 151: 107398. https://doi.org/10.1016/j.ymssp.2020.107398.
16. Mohammadi A, Westny T, Jung D, Krysander M. Analysis of numerical integration in RNN-based residuals for fault diagnosis of dynamic

systems. IFAC-PapersOnLine 2023; 56: 2909–2914. https://doi.org/10.1016/j.ifacol.2023.10.1411.
17. Wang H, Liu Z, Peng D, Cheng Z. Attention-guided joint learning CNN with noise robustness for bearing fault diagnosis and vibration signal denoising. ISA Transactions 2022; 128: 470–484. https://doi.org/10.1016/j.isatra.2021.11.028.
18. Guo P, Huang W, Jia N, Ding C, Huangfu Y, Jiang X, et al. A novel adaptive gating neurons model with physical features weighted for bearing fault diagnosis under strong noise. Engineering Applications of Artificial Intelligence 2025; 149: 110532. https://doi.org/10.1016/j.engappai.2025.110532.
19. Gawde S, Patil S, Kumar S, Kotecha K. A scoping review on multi-fault diagnosis of industrial rotating machines using multi-sensor data fusion. Artif Intell Rev 2023; 56: 4711–4764. https://doi.org/10.1007/s10462-022-10243-z.
20. Shao H, Lin J, Zhang L, Galar D, Kumar U. A novel approach of multisensory fusion to collaborative fault diagnosis in maintenance. Information Fusion 2021; 74: 65–76. https://doi.org/10.1016/j.inffus.2021.03.008.
21. Wu P, Nie X, Xie G. Multi-sensor signal fusion for a compound fault diagnosis method with strong generalization and noise-tolerant performance. Meas Sci Technol 2020; 32: 035108. https://doi.org/10.1088/1361-6501/abc6e3.
22. Ye M, Yan X, Hua X, Jiang D, Xiang L, Chen N. MRCFN: A multi-sensor residual convolutional fusion network for intelligent fault diagnosis of bearings in noisy and small sample scenarios. Expert Systems with Applications 2025; 259: 125214. https://doi.org/10.1016/j.eswa.2024.125214.
23. Yan X, Yan W-J, Xu Y, Yuen K-V. Machinery multi-sensor fault diagnosis based on adaptive multivariate feature mode decomposition and multi-attention fusion residual convolutional neural network. Mechanical Systems and Signal Processing 2023; 202: 110664. https://doi.org/10.1016/j.ymssp.2023.110664.
24. Wu Z, Pan S, Chen F, Long G, Zhang C, Yu P S. A Comprehensive Survey on Graph Neural Networks. IEEE Trans Neural Netw Learning Syst 2021; 32: 4–24. https://doi.org/10.1109/TNNLS.2020.2978386.
25. Scarselli F, Gori M, Ah Chung Tsoi, Hagenbuchner M, Monfardini G. The Graph Neural Network Model. IEEE Trans Neural Netw 2009; 20: 61–80. https://doi.org/10.1109/TNN.2008.2005605.
26. Liu J, Yuan X, Yang X, Zhu W, Zhang Y, Ye T, Yao X, Zhou F. MGTN-DSI: A multi-sensor graph transfer network considering dual structural information for fault diagnosis under varying working conditions. Advanced Engineering Informatics 2025; 65: 103119. https://doi.org/10.1016/j.aei.2025.103119.
27. Xu J, Ke H, Jiang Z, Mo S, Chen Z, Gui W. OHCA-GCN: A novel graph convolutional network-based fault diagnosis method for complex systems via supervised graph construction and optimization. Advanced Engineering Informatics 2024; 61: 102548. https://doi.org/10.1016/j.aei.2024.102548.
28. Wang L, Xie F, Zhang X, Jiang L, Huang B. Spatial-temporal graph feature learning driven by time–frequency similarity assessment for robust fault diagnosis of rotating machinery. Advanced Engineering Informatics 2024; 62: 102711. https://doi.org/10.1016/j.aei.2024.102711.
29. Li C, Mo L, Kwoh CK, Li X, Chen Z, Wu M, Yan R. Noise-robust multi-view graph neural network for fault diagnosis of rotating machinery. Mechanical Systems and Signal Processing 2025; 224: 112025. https://doi.org/10.1016/j.ymssp.2024.112025.
30. Liu Y, Yu Z, Xie M. Cascading time-frequency transformer and spatio-temporal graph attention network for rotating machinery fault diagnosis. IEEE Transactions on Instrumentation and Measurement 2024; 73: 1–10. https://doi.org/10.1109/TIM.2024.3453312.
31. Pang P, Tang J, Luo J, Chen M, Yuan H, Jiang L. An explainable and lightweight improved 1-D CNN model for vibration signals of rotating machinery. IEEE Sensors Journal 2024; 24: 6976–6997. https://doi.org/10.1109/JSEN.2023.3327783.
32. Kang S. k-nearest neighbor learning with graph neural networks. Mathematics 2021; 9: 830. https://doi.org/10.3390/math9080830.
33. Yang Y, Li T, Sun C, Zhang L, Yan R. Graph attention U-net to fuse multi-sensor signals for long-tailed distribution fault diagnosis. Engineering Applications of Artificial Intelligence 2023; 126: 106927. https://doi.org/10.1016/j.engappai.2023.106927.
34. Zhao C, Zio E, Shen W. Domain generalization for cross-domain fault diagnosis: An application-oriented perspective and a benchmark study. Reliability Engineering & System Safety 2024; 245: 109964. https://doi.org/10.1016/j.ress.2024.109964.
35. Li C, Mo L, Yan R. Rotating machinery fault diagnosis based on spatial-temporal GCN. 2021 International Conference on Sensing, Measurement & Data Analytics in the era of Artificial Intelligence (ICSMD), Nanjing, China: IEEE; 2021: 1–6. https://doi.org/10.1109/ICSMD53520.2021.9670851.

36. Veličković P, Cucurull G, Casanova A, Romero A, Liò P, Bengio Y. Graph Attention Networks 2018.
37. Zhu G, Liu X, Tan L. Bearing fault diagnosis based on sparse wavelet decomposition and sparse graph connection using GraphSAGE. 2023 IEEE 2nd International Conference on AI in Cybersecurity (ICAIC), Houston, TX, USA: IEEE; 2023: 1–6. https://doi.org/10.1109/ICAIC57335.2023.10044173.
38. Xu K, Hu W, Leskovec J, Jegelka S. How powerful are graph neural networks? 2019. https://doi.org/10.48550/arXiv.1810.00826.
39. Morris C, Ritzert M, Fey M, Hamilton WL, Lenssen JE, Rattan G, Grohe M. Weisfeiler and leman go neural: Higher-order graph neural networks 2021. https://doi.org/10.48550/arXiv.1810.02244.
40. Zhu D, Song X, Yang J, Cong Y, Wang L. A bearing fault diagnosis method based on L1 regularization transfer learning and LSTM deep learning. 2021 IEEE International Conference on Information Communication and Software Engineering (ICICSE), Chengdu, China: IEEE; 2021: 308–12. https://doi.org/10.1109/ICICSE52190.2021.9404081.